Dynamics of Vibratory Microgyroscopes. *

Scott R. Ploen †and David S. Bayard
Jet Propulsion Laboratory
California Institute of Technology
4800 Oak Grove Drive
Pasadena, CA 91009-8099

Abstract

In this report we provide a vectorial derivation of the equations of motion characterizing the dynamic behavior of both ideal and non-ideal (e.g., including anisoelastic effects) vibratory micromachined gyroscopes. The derivation presented here utilizes the basis-free Newton-Euler approach (viz., the balance of angular momentum) rather than an energy based formulation. Our approach offers the following advantages: (1) It leads to an explicit set of dynamic equations without requiring excessive symbolic manipulations by the analyst, (2) The resulting nonlinear dynamic model can be readily linearized for use in controller/estimator design, (3) Our derivation provides maximal physical insight into the dynamic behavior of micromachined rate sensors, (4) The Newton-Euler approach can can be readily extended to model multibody effects such as rotor/housing dynamic coupling. Although we emphasize the dynamic behavior of angularly vibrating microgyros in this report our formulation is equally valid for linearly vibrating microgyros.

1 Introduction

High performance gyroscopes are commonly used devices for measuring attitude and angular velocity in modern aerospace, vehicle, and robotic systems. The evolution of gyroscope technology (and more broadly inertial navigation technology) is an interesting topic in its own right - See [11] and [20] for a discussion and an extensive list of references. One of the earliest implementations of a device capable of sensing the angular rate of a rotating body (viz., the Earth) dates back to 1851 and Foucault's pendulum [13], [17]. In modern inertial sensor systems gyroscopes are typically classified as either rate gyros or rate integrating gyros [14]. In this report we will concentrate on the analysis of rate gyros; i.e., gyros that directly measure

*This research was performed at the Jet Propulsion Laboratory, Californ ia Institute of Technology, under contract with the National Aeronautics and Space Administratio n.

†Corresponding author - Email: sploen@grover.jpl.nasa.gov

the angular rate of a rotating body about a specific axis. Gyroscopes may be further categorized by their gross physical dimensions.[1] For example, the prototypical *macro* rate gyro consists of the classical single-axis deflection gyro (found in 3-axis stabilized platforms) incorporating a massive spinning rotor. The dynamic characteristics of macro rate gyros are well established - The reader should consult [13], [14] for further information. Alternately, recent MEMS (Micro-Electrical-Mechanical-System) technology has led to the reality of silicon-based monolithic micromachined (or *micro*) devices becoming viable low cost alternatives to their macro counterparts in a variety of lower performance applications. This revolution has increased the need to understand not only the dynamic behavior of these MEMS devices but also to develop the necessary architecture required to implement functionally integrated microgyro based sensor systems.

In this report we concentrate on developing dynamic models of microgyro devices for use in design, performance evaluation, and control. Specifically, we present a first principles derivation of the equations of motion for the important class of sensors known as *angularly vibrating rate microgyros.* The derivation given here utilizes the vectorial (basis-free) Newton-Euler approach (balance of angular momentum) rather than an energy based formulation as done in [9], [11], [21]. Our approach leads to an explicit set of dynamic equations without requiring excessive symbolic manipulations. Further, the derivation allows maximal physical insight into the dynamic operation of micromachined rate sensors and allows the analyst to naturally incorporate multibody effects (as well as other parasitic effects) into the analysis.

2 Dynamics of the Angularly Vibrating Rate Gyroscope

In this section we derive the equations of motion of a generic vibrating angular rate microgyro. The dynamic analysis of rotational vibratory gyroscopes is also discussed in [2], [9], [11], [19], and [21]. Before we begin developing the equations of motion of the microgyro we present a qualitative overview of the operation of the device. The configuration of the rate gyro under study is shown in Figure 1. The rotor is angularly oscillated about the z_p-axis (drive-axis, normal to the plane of the page) resulting in an oscillating angular momentum vector. The suspension system of the rotor consists of four cantilevered beams connecting the rotor structure to the gyro platform/housing assembly. The beams provide mechanical support and allow small angle flexure (via torsional motion) of the rotor relative to the platform about each axis[2]. If the spacecraft is rotating about the y_p-axis (input-axis) with some nonzero

[1]See [1] for a well written overview of both macro and micro vibratory rate gyros.

[2]The JPL angular rate microgyro structure is based on a similar configuration [4],[5],[12],[18],[21]. The microgyro consists of a four-leaf clover shaped plate rigidly coupled to a central mass element (called the post) mounted orthogonal to the plane of the clover leafs. The entire structure is suspended by four thin silicon cantilevered beams which provide mechanical support and restoring force/torque capability for the structure. The post axis is the input axis, and the drive and sense axes lie in the clover leaf plane. The dynamic model derived in this report can be readily applied

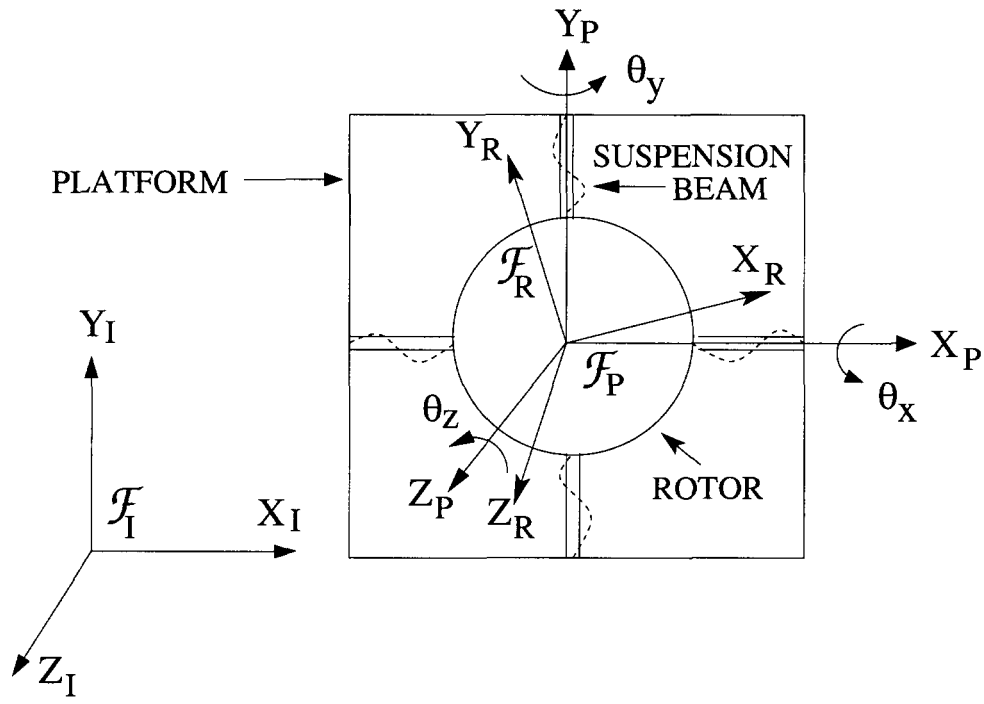

Figure 1: Angular Vibratory Rate Gyro

angular rate Ω_y (i.e., the rate to be sensed), an oscillating Coriolis moment is developed across the transverse x_p-axis (sense axis). This (fictitious) moment causes the rotor to be angularly deflected about the sense axis. The amplitude of the resulting angular deflection about the sense axis is directly related to the angular rate of the spacecraft about the input-axis. The description of gyro operation given here assumes that the gyro is operating in *open-loop* mode. The gyro can also be operated in a *closed-loop* mode that utilizes force rebalance along the $x-p$ and $y-p$ axes; In this mode of operation, rather than measuring the deflection about the sense axis directly, a torque is applied about the sense axis to null the Coriolis induced motion. The magnitude of the rebalancing torque is then directly related to the angular rate of the spacecraft.

2.1 Vectorial Equations of Motion

In the sequel the following reference frames shown in Figure 1 will play an important role:

- $\mathcal{F}_I$ - A suitable inertial frame of reference.
- $\mathcal{F}_P$ - The platform reference frame rigidly attached at the center of mass of the platform and rotating with the platform. In this analysis we will assume that relative motion between the platform and the vehicle is negligible - As a

to the specific geometry of the JPL clover-leaf gyro configuration by choosing the mass distribution accordingly.

result, the platform frame also describes the motion of the spacecraft (i.e., the platform frame can be taken equal to the spacecraft's body fixed frame $\mathcal{F}_B$).

- $\mathcal{F}_R$ - The rotor frame rigidly attached at the mass center of the rotor and rotating with the same angular motion of the rotor. The rotor can perform oscillations about the z_R axis. Note from Figure 1 that when the angular displacements $\theta_x = \theta_y = 0$, $\mathcal{F}_R$ is aligned with $\mathcal{F}_P$. This corresponds to the initial state of the device before a spacecraft rate induces rotational motion about the X_p (resp. Y_p) axis. Here we assume that the center of mass of the rotor and the platform coincide at point C. For simplicity we assume that the center of mass of the gyro *system* (rotor + platform + suspension) is also located at point C.

All dynamic coupling between the spacecraft and the microgyro is assumed to arise from the gross motion of the spacecraft; i.e., the gyro motion is dynamically coupled to the vehicle but not vise-versa[3]. As a result, the motion of the spacecraft will be taken as prescribed in this analysis. Furthermore, by the assumption that there exists no relative motion between the platform and the vehicle the motion of the platform can also be considered prescribed and the platform angular velocity is taken equal to the angular velocity of the spacecraft (i.e., the rate that we wish to sense). [4] The beams making up the rotor suspension assembly are modeled as lumped (i.e., massless) torsional spring/dashpot elements in the sequel. As a result the rotor suspension does not contribute angular momentum to the system.

Applying the balance of angular momentum [8] about the center of mass of the system (= center-of-mass of platform = center-of-mass of rotor) we find

$$\sum \vec{M} = \frac{{}^I d\vec{H}}{dt} \tag{1}$$

where

$$\begin{aligned} \vec{H} &= \vec{H}_R + \vec{H}_S && (2) \\ &\approx \vec{H}_R && (3) \\ &= \mathbf{J_R} \cdot {}^I\vec{\omega}^R && (4) \end{aligned}$$

Here $\vec{H}$ denotes the total angular momentum of the system (=rotor + suspension + platform) about the system center-of-mass, $\vec{H}_R$ denotes the angular momentum of the rotor about the system center of mass, and $\vec{H}_S$ denotes the angular momentum of the suspension about the system center-of-mass[5]. Also, $\mathbf{J}_R$ denotes the inertia dyadic of the rotor about its center of mass, ${}^I\vec{\omega}^R$ is the angular velocity of the rotor relative to $\mathcal{F}_I$, and $\sum \vec{M}$ denotes the resultant moment vector acting on the rotor. The symbol $\cdot$ represents dyad-vector multiplication [8]. Following the notation of

[3]Note that this assumption does not always hold for the analysis of macro-rate gyros incorporating a massive spinning rotor.

[4]For our purposes the concept of a prescribed motion can be best thought of as motion resulting from the action of a perfect (infinite bandwidth) control system.

[5]As the motion of the platform is taken as prescribed $\vec{H}_P$ is not included in the analysis.

[10], $\frac{^A d}{dt}(\bullet)$ denotes the time rate of change of a vector as seen by an observer rigidly attached to frame of reference A, denoted $\mathcal{F}_A$. In the analysis of a system involving multiple reference frames (undergoing arbitrary relative motion) the analyst must carefully distinguish between the time rates of change of vector/tensor quantities as seen by observers in different frames. Specifically, given a pair of reference frames $\mathcal{F}_A$ and $\mathcal{F}_B$ undergoing arbitrary relative angular motion, the time rate of change of a vector $\vec{Q}$ as seen by an observer rigidly fixed to $\mathcal{F}_A$ (denoted $\frac{^A d\vec{Q}}{dt}$) is related to the time rate of change of the *same vector* as seen by an observer rigidly fixed to $\mathcal{F}_B$ (denoted $\frac{^B d\vec{Q}}{dt}$) via the *transport theorem*

$$\frac{^A d\vec{Q}}{dt} = \frac{^B d\vec{Q}}{dt} + ^A\vec{\omega}^B \times \vec{Q} \tag{5}$$

where $^A\vec{\omega}^B$ denotes the angular velocity of frame B in (or relative to) frame A. For a detailed derivation of the transport theorem see [10] or [8].

Applying the transport theorem to the balance of angular momentum (1) we find

$$\frac{^I d\vec{H}}{dt} = \frac{^P d\vec{H}}{dt} + ^I\vec{\omega}^P \times \vec{H} \tag{6}$$

where $^I\vec{\omega}^P$ denotes the absolute angular velocity of frame P. Applying the transport theorem a second time to $\frac{^P d\vec{H}}{dt}$ results in

$$\frac{^P d\vec{H}}{dt} = \frac{^R d\vec{H}}{dt} + ^P\vec{\omega}^R \times \vec{H} \tag{7}$$

where $^P\vec{\omega}^R$ is the angular velocity of frame R in frame P. Note that two applications of the transport theorem are required since $\mathcal{F}_R$ is rotating relative to $\mathcal{F}_P$ and $\mathcal{F}_P$ is rotating relative to $\mathcal{F}_I$.

Substituting (7) into (6) and rearranging yields

$$\frac{^I d\vec{H}}{dt} = \frac{^R d\vec{H}}{dt} + (^I\vec{\omega}^P + ^P\vec{\omega}^R) \times \vec{H} \tag{8}$$

$$= \frac{^R d\vec{H}}{dt} + ^I\vec{\omega}^R \times \vec{H} \tag{9}$$

where in (9) we have invoked the *angular velocity addition theorem* (see [10])

$$^I\vec{\omega}^R = ^I\vec{\omega}^P + ^P\vec{\omega}^R \tag{10}$$

Equation (9) can be further simplified as follows

$$\frac{^R d\vec{H}}{dt} = \frac{^R d}{dt}(\mathbf{J_R} \cdot ^I\vec{\omega}^R) \tag{11}$$

$$= (\frac{^R d\mathbf{J_R}}{dt}) \cdot ^I\vec{\omega}^R + \mathbf{J_R} \cdot (\frac{^R d^I\vec{\omega}^R}{dt}) \tag{12}$$

However, since the rotor is assumed rigid (i.e., does not suffer any deformation) and $\mathcal{F}_R$ is rigidly attached to the rotor structure

$$\frac{{}^R d\mathbf{J_R}}{dt} = \mathbf{0} \tag{13}$$

Substituting (9), (12)-(13) into (6), it follows that the resulting vectorial of motion are expressed concisely as

$$\sum \vec{M} = \mathbf{J_R} \cdot \frac{{}^R d^I \vec{\omega}^R}{dt} + {}^I\vec{\omega}^R \times \mathbf{J_R} \cdot {}^I\vec{\omega}^R \tag{14}$$

It is also important to observe from applying the transport theorem to ${}^I\vec{\omega}^R$ that

$$\frac{{}^I d^I \vec{\omega}^R}{dt} = \frac{{}^R d^I \vec{\omega}^R}{dt} + {}^I\vec{\omega}^R \times {}^I\vec{\omega}^R \tag{15}$$

$$= \frac{{}^R d^I \vec{\omega}^R}{dt} \tag{16}$$

Some final comments on the Newton-Euler formulation are in order. For simplicity, we assumed that the rotor suspension is massless and have neglected all dynamic coupling between the platform and the rotor in this analysis. However, to obtain a more realistic dynamic model multibody coupling effects should be considered. In the field of multibody dynamics [8] the Newton-Euler method is the preferred method to formulate the equations of motion of interconnected systems of rigid-flexible bodies. As a result, our framework can be readily extended to incorporate platform/rotor multibody coupling effects.

2.2 Representation of the Equations of Motion in $\mathcal{F}_R$

The vectorial equation (14) along with the vectorial statement of the angular velocity relationship (10) and its time rate of change (16) provide a concise and *exact* characterization of the non-linear equations of motion of the microgyroscope[6].

Once a basis-free (i.e., vectorial) statement of the equations of motion of the system has been determined the analyst has complete freedom to express the equations in component form by resolving them into any reference frame of interest. In problems involving a single rigid body the natural frame to express the dynamics in component form is a body fixed frame rigidly attached to the body and rotating with the body. In the analysis of the microgyro this frame corresponds to $\mathcal{F}_R$[7]. To this end, we will seek a coordinate representation of (14) in $\mathcal{F}_R$. As intermediate steps we must first

[6] As discussed in the next section a kinematic differential equation relating ${}^I\vec{\omega}^R$ to the time rate of change of some specific parameterization of the rotation group (e.g., Euler angles, quaternions, etc.) is also required to completely characterize the state of the system.

[7] As remarked above, $\mathcal{F}_R$ has the property that the representation of $\mathbf{J}_R$ in this frame is constant. However, restoring moments from the elastic beam flexures are more naturally expressed in $\mathcal{F}_P$.

determine the representations of ${}^I\vec{\omega}^R$, $\frac{{}^I d^I\vec{\omega}^R}{dt}$, $\mathbf{J}_R$ and $\sum \vec{M}$ in $\mathcal{F}_R$[8]

As a first step in expressing the equations of motion in component form resolved in $\mathcal{F}_R$ we must describe the orientation of $\mathcal{F}_R$ relative to $\mathcal{F}_P$. Here the rotation matrix $C : \mathcal{F}_P \mapsto \mathcal{F}_R$ describing the attitude of $\mathcal{F}_R$ relative to $\mathcal{F}_P$ is parameterized via Euler angles - However, other parameter alternates are possible [8]. [9] Consider the following $(1, 2, 3)$ Euler sequence[10]

$$C = C_z(\theta_z)C_y(\theta_y)C_x(\theta_x) \tag{17}$$

where the *principal rotation matrices* are defined by

$$C_x(\theta_x) = \begin{bmatrix} 1 & 0 & 0 \\ 0 & \cos(\theta_x) & \sin(\theta_x) \\ 0 & -\sin(\theta_x) & \cos(\theta_x) \end{bmatrix} \tag{18}$$

$$C_y(\theta_y) = \begin{bmatrix} \cos(\theta_y) & 0 & -\sin(\theta_y) \\ 0 & 1 & 0 \\ \sin(\theta_y) & 0 & \cos(\theta_y) \end{bmatrix} \tag{19}$$

$$C_z(\theta_z) = \begin{bmatrix} \cos(\theta_z) & \sin(\theta_z) & 0 \\ -\sin(\theta_z) & \cos(\theta_z) & 0 \\ 0 & 0 & 1 \end{bmatrix} \tag{20}$$

The Euler angles $(\theta_x, \theta_y, \theta_z)$ correspond physically to small rotations about the sense-axis, input-axis, and drive axis respectively.

Expanding out (17) in terms of the principle rotation matrices we find

$$C = \begin{bmatrix} c\theta_y c\theta_z & s\theta_x s\theta_y c\theta_z + c\theta_x s\theta_z & -c\theta_x s\theta_y c\theta_z + s\theta_x s\theta_z \\ -c\theta_y s\theta_z & -s\theta_x s\theta_y s\theta_z + c\theta_x c\theta_z & c\theta_x s\theta_y s\theta_z + s\theta_x c\theta_z \\ s\theta_y & -s\theta_x c\theta_y & c\theta_x c\theta_y \end{bmatrix} \tag{21}$$

where $c\theta = \cos(\theta)$ and $s\theta = \sin(\theta)$.

[8]At this stage, we are tempted to introduce the notation ${}^AQ$ to denote the coordinate representations of an arbitrary vector $\vec{Q}$ in a reference frame $\mathcal{F}_A$. Here we are making the critical distinction between a geometric vector $\vec{Q}$ and its representation in a particular reference frame $\mathcal{F}_A$ as a column vector ${}^AQ \in \Re^3$. The vector $\vec{Q}$ is a geometric object and exists independent of any particular frame of reference. However, once we choose a preferred frame (viz., an orthonormal basis in linear algebra parlance) the underlying geometric vector admits a coordinate representation specific to our choice of frame. If we observe the *same* vector from a different frame (corresponding to a change of orthonormal basis) the coordinate representation will change accordingly. However, although the superscript notation makes the reference frame involved *explicit* in each equation, a price is paid in notational complexity as the equations will then contain *both* superscripts and subscripts; e.g. the angular velocity of frame R relative to frame P expressed in frame P would be denoted ${}^P({}^P\omega^R)$. To avoid a morass of indices we omit the leading superscript from column vectors and attempt to make clear from context the underlying reference frame(s) involved.

[9]The Euler angle parameterization of $SO(3)$ is particularly useful for gaining physical insight when small angle motion is involved.

[10]First perform a rotation about the x-axis by θ_x , followed by a rotation about the intermediate y-axis by θ_y, followed by a rotation about the final z-axis by θ_z.

Once the rotation matrix $C : \mathcal{F}_P \mapsto \mathcal{F}_R$ is known, the angular velocity of $\mathcal{F}_R$ relative to $\mathcal{F}_P$ *expressed in* $\mathcal{F}_R$ is given by (see [8])

$$
\begin{aligned}
[{}^P\omega^R] &:= -\dot{C}C^T && (22)\\
&= -\dot{C}_z C_z^T - C_z(\dot{C}_y C_y^T)C_z^T - C_z C_y(\dot{C}_x C_x^T)C_y^T C_z^T && (23)
\end{aligned}
$$

where

$$
[\omega] := \begin{bmatrix} 0 & -\omega_3 & \omega_2 \\ \omega_3 & 0 & -\omega_1 \\ -\omega_2 & \omega_1 & 0 \end{bmatrix} \tag{24}
$$

Denoting

$$
\begin{aligned}
[\omega_x] &:= -\dot{C}_x C_x^T && (25)\\
[\omega_y] &:= -\dot{C}_y C_y^T && (26)\\
[\omega_z] &:= -\dot{C}_z C_z^T && (27)
\end{aligned}
$$

and recalling the matrix identity

$$
C[\omega]C^T = [C\omega] \tag{28}
$$

where $C \in SO(3)$[11] we find

$$
[{}^P\omega^R] = -[\omega_z] - C_z[\omega_y]C_z^T - C_z C_y[\omega_x]C_y^T C_z^T \tag{29}
$$

or equivalently

$$
{}^P\omega^R = \omega_z + C_z\omega_y + (C_z C_y)\omega_x \tag{30}
$$

A straightforward calculation results in

$$
\begin{aligned}
\omega_x &= [\dot{\theta}_x,\ 0,\ 0]^T && (31)\\
\omega_y &= [0,\ \dot{\theta}_y,\ 0]^T && (32)\\
\omega_z &= [0,\ 0,\ \dot{\theta}_z]^T && (33)
\end{aligned}
$$

Combining (19)-(20) and (30)-(33) we find

$$
\begin{aligned}
{}^P\omega^R &= \begin{bmatrix} \dot{\theta}_x c\theta_y c\theta_z + \dot{\theta}_y s\theta_z \\ -\dot{\theta}_x c\theta_y s\theta_z + \dot{\theta}_y c\theta_z \\ \dot{\theta}_z + \dot{\theta}_x s\theta_y \end{bmatrix} && (34)\\
&= \begin{bmatrix} c\theta_y c\theta_z & s\theta_z & 0 \\ -c\theta_y s\theta_z & c\theta_z & 0 \\ s\theta_y & 0 & 1 \end{bmatrix} \begin{bmatrix} \dot{\theta}_x \\ \dot{\theta}_y \\ \dot{\theta}_z \end{bmatrix} && (35)\\
&= S(\Theta)\dot{\Theta} && (36)
\end{aligned}
$$

[11]Recall that $SO(3)$ denotes the *Special Orthogonal Group* of 3×3 orthogonal matrices of determinant $+1$.

where $\dot{\Theta} = [\dot{\theta}_x \ \dot{\theta}_y \ \dot{\theta}_z]^T$ and $S(\Theta)$ is as given in (35).

The angular velocity of the platform $\mathcal{F}_P$ relative to $\mathcal{F}_I$ (the rate we wish to sense) expressed in $\mathcal{F}_P$ is given by

$$^I\omega^P = [\Omega_x, \ \Omega_y, \ \Omega_z]^T \tag{37}$$

As discussed earlier, the angular velocity (and the associated angular acceleration) of the platform is treated as prescribed in this analysis and is taken equal to the angular velocity of the spacecraft.

Collecting the coordinate expression (37) and (36) it follows from the angular velocity addition theorem that $^I\vec{\omega}^R = ^P\vec{\omega}^R + ^I\vec{\omega}^P$; Expressed in $\mathcal{F}_R$ we find

$$^I\omega^R = S\dot{\Theta} + C \ ^I\omega^P \tag{38}$$

As anticipated $^I\omega^P$ (i.e., the representation of $^I\vec{\omega}^P$ in $\mathcal{F}_P$) must first be transformed to $\mathcal{F}_R$ via the rotation matrix C before being added to $^P\omega^R = S\dot{\Theta}$ (which is already resolved in $\mathcal{F}_R$).

From (16) we find that the absolute angular acceleration of the rotor $\frac{^Id^I\vec{\omega}^R}{dt}$ can be determined by differentiating the column matrix (38) with respect to time. We immediately find

$$^I\dot{\omega}^R = \dot{S}\dot{\Theta} + S\ddot{\Theta} + \dot{C} \ ^I\omega^P + C \ ^I\dot{\omega}^P \tag{39}$$

Noting $\dot{C} \ ^I\omega^P = (\dot{C}C^T)C \ ^I\omega^P$ and $[^P\omega^R] = -\dot{C}C^T$, it follows

$$^I\dot{\omega}^R = \dot{S}\dot{\Theta} + S\ddot{\Theta} - \left[^P\omega^R\right] C \ ^I\omega^P + C \ ^I\dot{\omega}^P \tag{40}$$

The resultant moment vector $\sum \vec{M}$ acting on the rotor is due to two sources (1) restoring torques and damping due to the suspension and (2) any applied torques such as control torques. Here we assume that all external torques (control + restoring + damping) are generated in the platform frame. Here we denote the components of $\sum \vec{M}$ in the platform frame $\mathcal{F}_P$ as $\sum M$; As a result, the representation of $\sum \vec{M}$ in $\mathcal{F}_R$ is given by $C \sum M$. The representation of the inertia tensor of the rotor $\mathbf{J}_R$ in $\mathcal{F}_R$ is denoted simply as J.

To summarize, the representation of the gyro equations of motion (14) in $\mathcal{F}_R$ is

$$J \ ^I\dot{\omega}^R + [^I\omega^R]J \ ^I\omega^R = C \sum M \tag{41}$$

where

$$^I\omega^R = S\dot{\Theta} + C \ ^I\omega^P \tag{42}$$

$$^I\dot{\omega}^R = \dot{S}\dot{\Theta} + S\ddot{\Theta} - \left[^P\omega^R\right] C \ ^I\omega^P + C \ ^I\dot{\omega}^P \tag{43}$$

Upon substituting the kinematic equations (42) and (43) into the balance of angular momentum (41) the nonlinear motion equations expressed in $\mathcal{F}_R$ take the form

$$J(\dot{S}\dot{\Theta} + S\ddot{\Theta} - \left[^P\omega^R\right] C \ ^I\omega^P + C \ ^I\dot{\omega}^P) + [S\dot{\Theta} + C \ ^I\omega^P]J(S\dot{\Theta} + C \ ^I\omega^P) = C \sum M \tag{44}$$

Note that the form of the resultant moment vector acting on the rotor must also be specified to obtain a complete description of the dynamics.

2.3 Small Angle Approximation of the Equations of Motion

Although (44) provides an explicit description of the nonlinear behavior of the device its complexity limits its utility for controller design[12]. Our present goal is to simplify the model (44) based on a small angle expansions of the kinematic relationships (42) and (43). This simplified model will provide far more insight in describing the operation of the gyroscope and further can be easily linearized for use in controller design. In the small angle approximation we will neglect all coupling between the Euler angles $(\theta_x, \theta_y, \theta_z)$ and their higher derivatives. However, we will retain terms consisting of products of the Euler angles $(\theta_x, \theta_y, \theta_z)$ and their derivatives with the spacecraft rates $(\Omega_x, \Omega_y, \Omega_z)$ and their derivatives.

To this end we first develop the small angle approximation of (42). Recalling for small θ $\sin(\theta) \approx \theta$ and $\cos(\theta) \approx 1$ we find

$$S\dot{\Theta} \approx \begin{bmatrix} 1 & \theta_z & 0 \\ -\theta_z & 1 & 0 \\ \theta_y & 0 & 1 \end{bmatrix} \begin{bmatrix} \dot{\theta}_x \\ \dot{\theta}_y \\ \dot{\theta}_z \end{bmatrix} \tag{45}$$

$$= \begin{bmatrix} \dot{\theta}_x + \theta_z\dot{\theta}_y \\ \dot{\theta}_y - \theta_z\dot{\theta}_x \\ \dot{\theta}_z + \theta_y\dot{\theta}_x \end{bmatrix} \tag{46}$$

$$\approx \begin{bmatrix} \dot{\theta}_x \\ \dot{\theta}_y \\ \dot{\theta}_z \end{bmatrix} \tag{47}$$

The orientation of the rotor relative to the platform (21) is approximated by

$$C \approx \begin{bmatrix} 1 & \theta_z & -\theta_y \\ -\theta_z & 1 & \theta_x \\ \theta_y & -\theta_x & 1 \end{bmatrix} \tag{48}$$

$$= I - [\Delta\Theta] \tag{49}$$

where

$$[\Delta\Theta] = \begin{bmatrix} 0 & -\theta_z & \theta_y \\ \theta_z & 0 & -\theta_x \\ -\theta_y & \theta_x & 0 \end{bmatrix} \tag{50}$$

As a consequence

$$C\,{}^I\omega^P \approx (I - [\Delta\Theta])^I\omega^P \tag{51}$$

$$= \begin{bmatrix} \Omega_x + \theta_z\Omega_y - \theta_y\Omega_z \\ \Omega_y + \theta_x\Omega_z - \theta_z\Omega_x \\ \Omega_z + \theta_y\Omega_x - \theta_x\Omega_y \end{bmatrix} \tag{52}$$

[12]However, it does provide an adequate truth model for testing and validating control designs.

Substituting the small angle approximations (47) and (52) into (42) results in

$$
{}^I\omega^R \approx \begin{bmatrix} \dot{\theta}_x + \Omega_x + \Omega_y\theta_z - \Omega_z\theta_y \\ \dot{\theta}_y + \Omega_y + \Omega_z\theta_x - \Omega_x\theta_z \\ \dot{\theta}_z + \Omega_z + \Omega_x\theta_y - \Omega_y\theta_x \end{bmatrix} \tag{53}
$$

The next step is to develop a small angle approximation for ${}^I\dot{\omega}^R$. In general, this should be accomplished by first explicitly computing ${}^I\dot{\omega}^R$ as given in (43) and then invoking the small angle approximation. However, since we are only interested in terms consisting of products of the Euler angles and the spacecraft rates it is possible to determine ${}^I\dot{\omega}^R$ to the required order by directly differentiating the small angle approximation of ${}^I\omega^R$ in (53). We immediately find

$$
{}^I\dot{\omega}^R \approx \begin{bmatrix} \ddot{\theta}_x + \dot{\Omega}_x + \dot{\Omega}_y\theta_z - \dot{\Omega}_z\theta_y + \Omega_y\dot{\theta}_z - \Omega_z\dot{\theta}_y \\ \ddot{\theta}_y + \dot{\Omega}_y + \dot{\Omega}_z\theta_x - \dot{\Omega}_x\theta_z + \Omega_z\dot{\theta}_x - \Omega_x\dot{\theta}_z \\ \ddot{\theta}_z + \dot{\Omega}_z + \dot{\Omega}_x\theta_y - \dot{\Omega}_y\theta_x + \Omega_x\dot{\theta}_y - \Omega_y\dot{\theta}_x \end{bmatrix} \tag{54}
$$

To simplify matters we will assume that $\mathcal{F}_\mathcal{R}$ is aligned with the principle axes of the rotor. As a result the inertia matrix of the rotor J is diagonal,

$$
J = Diag[J_{xx},\ J_{yy},\ J_{zz}] \tag{55}
$$

Under the principal axis assumption the rotational equations of motion (41) are known as *Euler's equations.* Expressed in $\mathcal{F}_R$ Euler's equations take the form

$$
\begin{aligned}
M_x &= J_{xx}\dot{\omega}_x + (J_{zz} - J_{yy})\omega_y\omega_z && (56)\\
M_y &= J_{yy}\dot{\omega}_y + (J_{xx} - J_{zz})\omega_x\omega_z && (57)\\
M_z &= J_{zz}\dot{\omega}_z + (J_{yy} - J_{xx})\omega_x\omega_y && (58)
\end{aligned}
$$

For simplicity we have introduced $\omega =^I \omega^R$ where the components of ω in $\mathcal{F}_R$ are denoted $(\omega_x,\ \omega_y,\ \omega_z)$ and the components of $\dot{\omega} = \dot{\omega}_{R/I}$ in $\mathcal{F}_R$ are denoted $(\dot{\omega}_x,\ \dot{\omega}_y,\ \dot{\omega}_z)$. Further the representation of $\sum \vec{M}$ in $\mathcal{F}_R$ (i.e., $C\sum M$) is denoted as $(M_x,\ M_y,\ M_z)$.

Grouping together the linearized kinematic equations (53) and (54) we find

$$
\begin{aligned}
\omega_x &\approx \dot{\theta}_x + \Omega_x + \Omega_y\theta_z - \Omega_z\theta_y && (59)\\
\omega_y &\approx \dot{\theta}_y + \Omega_y + \Omega_z\theta_x - \Omega_x\theta_z && (60)\\
\omega_z &\approx \dot{\theta}_z + \Omega_z + \Omega_x\theta_y - \Omega_y\theta_x && (61)
\end{aligned}
$$

and

$$
\begin{aligned}
\dot{\omega}_x &\approx \ddot{\theta}_x + \dot{\Omega}_x + \dot{\Omega}_y\theta_z - \dot{\Omega}_z\theta_y + \Omega_y\dot{\theta}_z - \Omega_z\dot{\theta}_y && (62)\\
\dot{\omega}_y &\approx \ddot{\theta}_y + \dot{\Omega}_y + \dot{\Omega}_z\theta_x - \dot{\Omega}_x\theta_z + \Omega_z\dot{\theta}_x - \Omega_x\dot{\theta}_z && (63)\\
\dot{\omega}_z &\approx \ddot{\theta}_z + \dot{\Omega}_z + \dot{\Omega}_x\theta_y - \dot{\Omega}_y\theta_x + \Omega_x\dot{\theta}_y - \Omega_y\dot{\theta}_x && (64)
\end{aligned}
$$

Upon substituting (59)-(64) into Euler's equations (56)-(58) and retaining terms involving products of the Euler angles (and their time derivatives) with the spacecraft

rates (and their time derivatives) we find

$$
\begin{aligned}
M_x &= J_{xx}\ddot{\theta}_x + J_{xx}\dot{\Omega}_x + (J_{xx} - J_{yy})\Omega_y\dot{\theta}_z + \theta_z[J_{xx}\dot{\Omega}_y + (J_{yy} - J_{zz})\Omega_x\Omega_z] \\
&\quad +(J_{zz} - J_{yy})\Omega_y\Omega_z + \theta_x(J_{zz} - J_{yy})(\Omega_z^2 - \Omega_y^2) \\
&\quad +(J_{zz} - J_{yy} - J_{xx})\Omega_z\dot{\theta}_y + \theta_y[-J_{xx}\dot{\Omega}_z + (J_{zz} - J_{yy})\Omega_x\Omega_y] + J_{zz}\Omega_y\dot{\theta}_z \quad (65) \\
M_y &= J_{yy}\ddot{\theta}_y + J_{yy}\dot{\Omega}_y + (J_{xx} - J_{yy})\Omega_x\dot{\theta}_z + \theta_x[J_{yy}\dot{\Omega}_z + (J_{zz} - J_{xx})\Omega_x\Omega_y] \\
&\quad +(J_{xx} - J_{zz})\Omega_x\Omega_z + \theta_y(J_{xx} - J_{zz})(\Omega_x^2 - \Omega_z^2) \\
&\quad +(J_{xx} - J_{zz} + J_{yy})\Omega_z\dot{\theta}_x + \theta_z[-J_{yy}\dot{\Omega}_x + (J_{xx} - J_{zz})\Omega_y\Omega_z] - J_{zz}\Omega_x\dot{\theta}_z \quad (66) \\
M_z &= J_{zz}\ddot{\theta}_z + J_{zz}\dot{\Omega}_z + (J_{yy} - J_{zz})\Omega_y\dot{\theta}_x + \theta_y[J_{zz}\dot{\Omega}_x - (J_{yy} - J_{xx})\Omega_y\Omega_z] \\
&\quad +(J_{yy} - J_{xx})\Omega_x\Omega_y + \theta_z(J_{yy} - J_{xx})(\Omega_y^2 - \Omega_x^2) \\
&\quad +(J_{yy} - J_{xx} + J_{zz})\Omega_x\dot{\theta}_y + \theta_x[-J_{zz}\dot{\Omega}_y + (J_{yy} - J_{xx})\Omega_x\Omega_z] - J_{xx}\Omega_y\dot{\theta}_x \quad (67)
\end{aligned}
$$

We assume that the rotor is symmetric about the x and y axes so that $J_{xx} = J_{yy}$. Further, we assume that both the principal axes of elasticity and damping of the suspension (i) coincide with each other, and (ii) align perfectly with $\mathcal{F}_P$. Under these assumptions the resultant moment about the center of mass of the system can be expressed in $\mathcal{F}_P$ as

$$
\sum M = \begin{bmatrix} -k_{xx}\theta_x - c_{xx}\dot{\theta}_x + M_x^e \\ -k_{yy}\theta_y - c_{yy}\dot{\theta}_y + M_y^e \\ -k_{zz}\theta_z - c_{zz}\dot{\theta}_z + M_z^e \end{bmatrix} \quad (68)
$$

Here, the restoring torques due to stiffness and damping along axis $i = (x, y, z)$ of $\mathcal{F}_P$ are denoted as $k_{ii}\theta_i$ and $c_{ii}\dot{\theta}_i$ respectively, and the components of the external moment acting about axis $i = (x, y, z)$ are denoted M_i^e. The restoring moments about each axis in (68) are decoupled due to assumptions (i) and (ii) above. Although this *isoelastic* assumption leads to a great simplification in the dynamic model, most real devices exhibit some form of *anisoelaticity* [4], [5]. We will further discuss this issue in the sequel.

The components of the moment vector $\sum M$ resolved in $\mathcal{F}_R$ are then

$$
\begin{aligned}
C\sum M &\approx (I - [\Delta\Theta])\sum M \quad (69) \\
&\approx \sum M \quad (70)
\end{aligned}
$$

Here we have neglected all products of the moments with the small angles (θ_x, θ_y, θ_z) in (70).

Substituting $J_{xx} = J_{yy}$ along with (68) into (65)-(67) and collecting terms yields

$$
\begin{aligned}
M_x^e &= J_{xx}\ddot{\theta}_x + c_{xx}\dot{\theta}_x + k_{xx}\theta_x + J_{xx}\dot{\Omega}_x + \theta_z[J_{xx}\dot{\Omega}_y + (J_{yy} - J_{zz})\Omega_x\Omega_z] \\
&\quad +(J_{zz} - J_{yy})\Omega_y\Omega_z + \theta_x(J_{zz} - J_{yy})(\Omega_z^2 - \Omega_y^2) \\
&\quad +(J_{zz} - J_{yy} - J_{xx})\Omega_z\dot{\theta}_y + \theta_y[-J_{xx}\dot{\Omega}_z + (J_{zz} - J_{yy})\Omega_x\Omega_y] + J_{zz}\Omega_y\dot{\theta}_z \quad (71) \\
M_y^e &= J_{yy}\ddot{\theta}_y + c_{yy}\dot{\theta}_y + k_{yy}\theta_y + J_{yy}\dot{\Omega}_y + \theta_x[J_{yy}\dot{\Omega}_z + (J_{zz} - J_{xx})\Omega_x\Omega_y] \\
&\quad +(J_{xx} - J_{zz})\Omega_x\Omega_z + \theta_y(J_{xx} - J_{zz})(\Omega_x^2 - \Omega_z^2) \\
&\quad +(J_{xx} - J_{zz} + J_{yy})\Omega_z\dot{\theta}_x + \theta_z[-J_{yy}\dot{\Omega}_x + (J_{xx} - J_{zz})\Omega_y\Omega_z] - J_{zz}\Omega_x\dot{\theta}_z \quad (72)
\end{aligned}
$$

$$M_z^e = J_{zz}\ddot{\theta}_z + c_{zz}\dot{\theta}_z + k_{zz}\theta_z + J_{zz}\dot{\Omega}_z + J_{zz}\theta_y\dot{\Omega}_x - J_{zz}\theta_x\dot{\Omega}_y + J_{zz}\Omega_x\dot{\theta}_y - J_{zz}\Omega_y\dot{\theta}_x \tag{73}$$

The simplified equations (71)-(73) exhibit the most important dynamic characteristics of the angularly vibrating microgyro. Specifically, the individual terms in (71)-(73) can be categorized as follows:

- The desired Coriolis coupling terms $J_{zz}\dot{\theta}_z\Omega_y$ and $-J_{zz}\dot{\theta}_z\Omega_x$.
- The undesired cross axis sensitivities involving terms of the form $\dot{\theta}_x\Omega_z$, $\theta_z\Omega_y\Omega_z$, etc.
- The undesired angular acceleration terms involving $(\dot{\Omega}_x,\ \dot{\Omega}_y,\ \dot{\Omega}_z)$.

For development of a control design model we neglect all cross-axis coupling and angular acceleration effects; It follows from (71)-(73) that the equations of motion are approximated by the following linear model

$$J_{xx}\ddot{\theta}_x + c_{xx}\dot{\theta}_x + k_{xx}\theta_x = -J_{zz}\dot{\theta}_z\Omega_y + M_x^e \tag{74}$$

$$J_{yy}\ddot{\theta}_y + c_{yy}\dot{\theta}_y + k_{yy}\theta_y = J_{zz}\dot{\theta}_z\Omega_x + M_y^e \tag{75}$$

$$J_{zz}\ddot{\theta}_z + c_{zz}\dot{\theta}_z + k_{zz}\theta_z = M_z^e \tag{76}$$

Dividing each equation (74)-(76) by the inertia about each respective axis transforms the dynamics to standard second order form

$$\ddot{\theta}_x + \frac{\omega_{xn}}{Q_x}\dot{\theta}_x + \omega_{xn}^2\theta_x = -\frac{J_{zz}}{J_{xx}}\dot{\theta}_z\Omega_y + \frac{M_x^e}{J_{xx}} \tag{77}$$

$$\ddot{\theta}_y + \frac{\omega_{yn}}{Q_y}\dot{\theta}_y + \omega_{yn}^2\theta_y = \frac{J_{zz}}{J_{yy}}\dot{\theta}_z\Omega_x + \frac{M_y^e}{J_{yy}} \tag{78}$$

$$\ddot{\theta}_z + \frac{\omega_{zn}}{Q_z}\dot{\theta}_z + \omega_{zn}^2\theta_z = \frac{M_z^e}{J_{zz}} \tag{79}$$

where the natural frequencies are $\omega_{in} = \sqrt{\frac{k_{ii}}{J_{ii}}}$ and the *quality factor* $Q_i = \frac{1}{2\zeta_i}$ where ζ_i denotes the damping ratio associated with axis $i = (x, y, z)$. The linear model (77)-(79) is well suited for use as a control design model [11].

We now revisit the principles of operation of the angularly vibrating microgyro in light of the linear model (77)-(79). First, a control loop is designed to command the external moment $M_z^e(t)$ in such a way that the steady state motion along the drive axis (z-axis) is given by

$$\theta_z(t) = Z_o cos(\omega_{zn}t) \tag{80}$$

Note that an oscillating momentum vector of magnitude $J_{zz}\dot{\theta}_z$ and circular frequency ω_{zn} is created along the drive axis[13]. Recall from (79) that the motion along the drive axis is completely decoupled (to first order) from the motion in the input/sense plane.

[13]Here we are assuming that the drive frequency ω_{zd} is equal to the natural frequency along the drive axis ω_{zn}.

As a result, the angular motion of the gyro along the z-axis will be taken as *prescribed* in following discussion. We further assume that the gyro is operating in *open loop* mode as described earlier in the other two axes. As a result we set $M_x^e = M_y^e = 0$. If the spacecraft begins to rotate about the input axis (y-axis) a Coriolis moment is developed along the sense axis (x-axis)[14]. The angular deflection along the x-axis is then governed by

$$\ddot{\theta}_x + \frac{\omega_{xn}}{Q_x}\dot{\theta}_x + \omega_{xn}^2\theta_x = \frac{J_{zz}}{J_{xx}} Z_o \omega_{zn}\Omega_y \sin(\omega_{zn}t) \tag{81}$$

Note that we have differentiated (80) and substituted the result into (77) to obtain (81). By using the Laplace transform it can be shown that the steady state solution to the LTI system (81) is

$$\theta_x^{ss}(t) = \frac{\frac{J_{zz}}{J_{xx}} Z_o \omega_{zn}\Omega_y}{\sqrt{(\omega_{xn}^2 - \omega_{zn}^2) + (\frac{\omega_{xn}\omega_{zn}}{Q_x})^2}} \sin(\omega_{zn}t - \phi_x) \tag{82}$$

$$= X_o \sin(\omega_{zn}t - \phi_x) \tag{83}$$

where the amplitude is given by

$$X_o = \frac{\frac{J_{zz}}{J_{xx}} Z_o \omega_{zn}\Omega_y}{\sqrt{(\omega_{xn}^2 - \omega_{zn}^2) + (\frac{\omega_{xn}\omega_{zn}}{Q_x})^2}} \tag{84}$$

and ϕ_x denotes the phase angle. In *open loop* mode the amplitude of the steady-state angular deflection about the x-axis is used to provide a measure of the spacecraft angular rate about the y-axis (input axis). This follows immediately by inspection of (84) where

$$|X_o| = \frac{|\frac{J_{zz}}{J_{xx}} Z_o \omega_{zn}\Omega_y|}{\sqrt{(\omega_{xn}^2 - \omega_{zn}^2) + (\frac{\omega_{xn}\omega_{zn}}{Q_x})^2}} \tag{85}$$

or

$$|\frac{X_o}{Z_o}| = \frac{|\frac{J_{zz}}{J_{xx}} \omega_{zn}\Omega_y|}{\sqrt{(\omega_{xn}^2 - \omega_{zn}^2) + (\frac{\omega_{xn}\omega_{zn}}{Q_x})^2}} \tag{86}$$

For maximum sensitivity of the device the natural frequency of the drive axis ω_{zn} and sense axes ω_{xn} should coincide. From symmetry of the device it automatically follows that $\omega_{xn} \approx \omega_{yn}$. However, the natural frequency of the drive axis (z-axis) must be forced to match the sense frequency by designing the suspension correctly. As pointed out in [11] it is difficult to passively design the housing/suspension to meet this requirement. Instead, a feedback control loop is required to regulate the oscillations along the drive axis in both magnitude and frequency. To this end, we assume that via proper design and/or control action along the drive axis the natural frequencies

[14]The device equations are symmetric about the x and y axes - As a result, either the x or y axis can be designated as the input axis. (resp. sense axis)

are approximately matched; i.e., $\omega_{xn} \approx \omega_{yn} \approx \omega_{zn}$. This common frequency will simply be denoted ω_n. Assuming matched frequencies it follows from (86) that

$$|\frac{X_o}{Z_o}| = \frac{|\frac{J_{zz}}{J_{xx}}\Omega_y Q_x|}{\omega_n} \tag{87}$$

The angular rate Ω_y can then be estimated by rearranging (87) to obtain

$$|\Omega_y| = \frac{\omega_n}{Q_x}\frac{J_{xx}}{J_{zz}}|\frac{X_o}{Z_o}| \tag{88}$$

Equation (88) is the key expression underlying the operation of the microgyro device.

As discussed earlier most real microgyro devices exhibit a certain amount of anisoelasticity due to imperfections introduced during fabrication[15]. Anisoelastic effects result in generalized coordinate coupling in the linear model. For example, consider the following model of the dynamics in the input/sense plane of a typical nonideal gyro

$$J_{xx}\ddot{\theta}_x + J_{xy}\ddot{\theta}_y + J_{xz}\ddot{\theta}_z + c_{xx}\dot{\theta}_x + c_{xy}\dot{\theta}_y + c_{xz}\dot{\theta}_z + k_{xx}\theta_x + k_{xy}\theta_y + k_{xz}\theta_z = -J_{zz}\dot{\theta}_z\Omega_y \tag{89}$$

$$J_{yx}\ddot{\theta}_x + J_{yy}\ddot{\theta}_y + J_{yz}\ddot{\theta}_z + c_{yx}\dot{\theta}_x + c_{yy}\dot{\theta}_y + c_{xz}\dot{\theta}_z + k_{yx}\theta_x + k_{yy}\theta_y + k_{yz}\theta_x = J_{zz}\dot{\theta}_z\Omega_x \tag{90}$$

To gain insight into the behavior of a nonideal (anisoelastic) device we will neglect all terms in (89) except for the damping coupling between the drive and sense axes. As a result,

$$J_{xx}\ddot{\theta}_x + c_{xx}\dot{\theta}_x + c_{xz}\dot{\theta}_z + k_{xx}\theta_x = -J_{zz}\dot{\theta}_z\Omega_y \tag{91}$$

or

$$J_{xx}\ddot{\theta}_x + c_{xx}\dot{\theta}_x + k_{xx}\theta_x = -(J_{zz}\Omega_y + c_{xz})\dot{\theta}_z \tag{92}$$

Notice that since $\dot{\theta}_z$ is assumed prescribed, c_{xz} now behaves as a *forcing term* in (92). As a result, even if $\Omega_y = 0$ (zero spacecraft rate) the sense axis will be angularly driven leading to a non-zero rate output. This situation is highly undesirable. Techniques to minimize and correct for anisoelastic effects are current research topics in the field of MEMS - See [16], [4], [5] for additional information.

3 Conclusions

In this report we have presented a first principles vectorial derivation of the equations of motion of both ideal and non-ideal (e.g., including anisoelastic effects) angularly vibrating micromachined gyroscopes. Our derivation utilized the basis-free Newton-Euler approach (viz., the balance of angular momentum) rather than more commonly used energy based formulations. Our basis-free approach to modeling leads to an

[15]Specifically, the principal axes of inertia, stiffness, and damping are not aligned with each other or with the frames $\mathcal{F}_R$ and $\mathcal{F}_P$.

explicit set of dynamic equations without requiring excessive symbolic manipulations by the analyst. The resulting nonliner dynamic model was then resolved inthe rotor frame of the gyro-assembly and simplified in order to gain insight into the physical operation of the device. The resulting linear model is well-suited for use in control and estimator design. Moreover, the Newton-Euler approach described here can can be readily extended to model multibody effects such as rotor/housing dynamic coupling.

References

[1] J.S. Burdess, A.J. Harris, J. Cruickshank, D. Wood, and G. Cooper, "A review of vibratory gyroscopes," *Engineering Science and Education Journal.* pp. 249-254, December 2000.

[2] T. Cai, "Dynamics of micromachined vibrating gimbal and wheel gyroscopes," *Communications in Nonlinear Science and Numerical Simulation.* Vol. 5, No. 2, pp. 45-48, 2000.

[3] B. Friedland, and M.F. Hutton, "Theory and error analysis of vibrating-member gyroscope," *IEEE Trans. Automatic Control* Vol. AC-23, No. 4, pp. 545-556, August 1978.

[4] K. Hayworth, "Derivation of closed loop scale factor, rate bias, and quadrature bias," *JPL Internal Document.*, January 2001.

[5] K. Hayworth, "Micro inertial reference system," *JPL Internal Document.*, September 2000.

[6] Y.S. Hong, J.H. Lee, and S.H. Kim, "A laterally driven symmetric micro-resonator for gyroscopic applications," *J. Micromech. Microeng.* Vol. 10, pp. 452-458, 2000.

[7] R. Horowitz, Y. Li, and S. Park, "Mechatronics of electrostatic microactuators and micro-gyroscopes," *Proc. of the 6th Int. Workshop on Advanced Motion Control.* pp. xxxi-xxxviii, March 30-April 1, 2000.

[8] P.C. Hughes, *Spacecraft Attitude Dynamics.* John Wiley, New York: 1986.

[9] T.N. Juneau, *Micromachined Dual Input Axis Rate Gyroscope.* Ph.D. Thesis, Dept. of Mechanical Engineering, University of California at Berkeley, 1997.

[10] T.R. Kane, and D.A. Levinson, *Dynamics: Theory and Applications.* McGraw-Hill, New York, 1985.

[11] P.B. Ljung, *Micromachined Gyroscope With Integrated Electronics.* Ph.D. Thesis, Dept. of Mechanical Engineering, University of California at Berkeley, 1997.

[12] R.T. M'Closkey, S. Gibson, and J. Hui, "Input-output dynamics of the JPL microscope," *Proc. of the IEEE Conf. on Decision and Control.* Tampa, FL, pp. 4328-4333, 1998.

[13] L. Meirovitch, *Methods of Analytical Dynamics.* McGraw-Hill, New York, 1970.

[14] S. Merhav, *Aerospace Sensor Systems and Applications.* Springer-Verlag, New York, 1996.

[15] A.M. Shkel, R. Horowitz, A.A. Seshia, S. Park, and R.T. Howe, "Dynamics and control of micromachined gyroscopes," *Proc. of the American Control Conference.* San Diego, CA, pp. 2119-2124, 1999.

[16] A. Shkel, R.T. Howe, and R. Horowitz, "Modeling and simulation of micromachined gyroscopes in the presence of imperfections," *Int. Conf. on Modeling and Simulation of Microsystems.* Puerto Rico, pp. 605-608, April 1999.

[17] J.L. Synge, and B.A. Griffith, *Principles of Mechanics, 3rd Edition.* McGraw-Hill, New York, 1959.

[18] T.K. Tang, R.C. Gutierrez, J.Z. Wilcox, et. al., "Silicon bulk micromachined vibratory gyroscope for microspacecraft," *Proc. of the SPIE - The International Society for Optical Engineering.* Vol. 2879, pp. 26-36, 1996.

[19] D. Teegarden, G. Lorenz, and R. Nuel, "How to model and simulate microgyroscope systems," *IEEE Spectrum.*, pp. 66-75, July 1998.

[20] D.H. Titterton, and J.L. Weston, *Strapdown Inertial Navigation Technology.* Peter Peregrinus Ltd., London, 1997.

[21] J.Z. Wilcox, "Cloverleaf vibratory gyroscope: dynamics and design," *JPL Interoffice Memorandum 1995-95-346.7-95*, November, 1995.